THE ASTRONOMICAL JOURNAL, 121:2515–2523, 2001 May
© 2001. The American Astronomical Society. All rights reserved. Printed in U.S.A.

HYDRODYNAMIC SIMULATIONS FOR THE NUCLEAR MORPHOLOGY OF NGC 4314

H. B. ANN
Department of Earth Sciences, Pusan National University, Pusan 609-735, Korea; hbann@cosmos.es.pusan.ac.kr
Received 2000 August 11; accepted 2001 January 16

ABSTRACT

We performed smoothed particle hydrodynamic (SPH) simulations to study the nuclear morphology of the barred galaxy NGC 4314. We have constructed the mass models based on the results of a profile decomposition into disk, bulge, and bar components. Our models have three different nuclear structures according to the assumption about the nuclear bar: no nuclear bar, a synchronous nuclear bar, and a fast nuclear bar. Our SPH simulations show that the morphology of the nuclear region of NGC 4314, which is characterized by an elongated ring and/or spiral of newly formed stars and H II regions, aligned nearly parallel to the primary bar, can be understood in terms of the secular evolution driven by the nonaxisymmetric potential. The slightly elongated and aligned nuclear ring of NGC 4314 can be formed by the strong barred potential and the moderate central concentration of the bulge mass, with and without a nuclear bar. However, the nuclear spiral pattern cannot be developed without a nuclear bar. The nuclear bar of NGC 4314 seems to rotate faster than the primary bar, since the nuclear morphology induced by the synchronous nuclear bar is much different from the observed one.

Key words: galaxies: individual (NGC 4314) — galaxies: nuclei — galaxies: structure — methods: numerical

1. INTRODUCTION

The nuclear ring of the barred spiral galaxy NGC 4314 has been studied extensively because of its peculiar morphology in the nuclear region, as clearly shown in the Hubble atlas (Sandage 1961). Earlier photometric studies showed that the color of the nuclear ring is bluer than that of the surrounding regions, including the nucleus (Lynds, Furenlid, & Rubin 1973; Benedict 1980). The blue color of the nuclear ring has been ascribed to the young stellar populations that might have formed from the disk material driven into a nuclear region by the bar potential (García-Barreto et al. 1991; Benedict et al. 1992, 1993; Benedict, Smith, & Kenny 1996). The presence of the young stellar populations in the nuclear region of NGC 4314 was suggested by the emission lines in the central region (Burbidge & Burbidge 1962; Wakamatsu & Nishida 1980) and the nuclear spirals in the center of the bar (Lynds 1974; Benedict 1980). Recent *Hubble Space Telescope* (*HST*) images of NGC 4314 clearly show that the nuclear ring is a nuclear spiral that consists of recently formed star clusters and H II regions (Benedict et al. 1993).

Thanks to extensive numerical studies, we are beginning to understand the formation and evolution of nuclear rings in barred galaxies. The presence of the inner Lindblad resonances (ILRs) is required for the formation of a nuclear ring (Schwarz 1981, 1984; Combes & Gerin 1985). The gravitational torque of the bar on the gas induces gas inflow, which leads to the formation of a nuclear ring at ILRs (Combes 1996). Because the shape and orientation of a nuclear ring depend on the dynamical properties of a galaxy (Combes & Gerin 1985; Athanassoula 1992; Piner, Stone, & Teuben 1995; Ann & Lee 2000), we can use the morphology of a nuclear ring, combined with hydrodynamic simulations, as a probe of the underlying dynamics. A general analysis of gas responses to bar forcing in disk galaxies is given by Ann & Lee (2000).

NGC 4314 seems to be a classic example of a barred galaxy, whose bar drives disk gas into a ring at ILRs. We aim to analyze the morphology and dynamics of the central region of NGC 4314 by smoothed particle hydrodynamic (SPH) simulations. In § 2, we describe the global and nuclear morphology of NGC 4314. Models of the present simulations are presented in § 3, and the results of the SPH simulations are described in § 4. Discussion on the nuclear ring morphology and nuclear bar is given in § 5, and the conclusions are given in the last section.

2. MORPHOLOGY

2.1. *Global Morphology*

NGC 4314 is an early-type barred galaxy, classified as SBa. The global morphology of NGC 4314 is characterized by a prominent bar and a peculiar bulge with faint outer spiral arms. There are many photographs and CCD images in the literature that show the general morphology of NGC 4314, but the global morphology is best seen in the Hubble atlas (Sandage 1961). NGC 4314 is a nearly face-on galaxy, with inclination of about 23°. The bulge is somewhat elongated along the bar, and it seems to be triaxial because it shows isophotal twists. The length, axial ratio, and position angle of the bar are $\sim 66''$, ~ 4, and $\sim 148°$, respectively (Benedict et al. 1996; Ann 1999). Because the position angle of the major axis of the disk is about 59° (Benedict et al. 1996), the bar aligns almost perpendicular to the disk. The outer spiral arms are very faint, but they trace 130° arcs out to $125''$ from the nucleus (García-Barreto et al. 1991). There seems to be no H II region in the outer arms (Burbidge & Burbidge 1962). The faintness of the outer spiral arms is due to the lack of gas (Gallagher, Faber, & Balick 1975; García-Barreto et al. 1991), which prevents recent star formation in the outer disk. However, the main three components, that is, disk, bulge, and bar, have comparable luminosities (Ann 1999).

2.2. *Nuclear Morphology*

NGC 4314 has been known to have a peculiar morphology in the central part of the galaxy (Sandage 1961). Earlier studies of NGC 4314 (Benedict 1980; García-Barreto et al. 1991; Benedict et al. 1992, 1993) showed a nuclear ring and

nuclear spiral pattern, along with several hot spots in the nuclear region. Figure 1 shows a deprojected gray-scale image of the nuclear region of NGC 4314 captured by *HST* NICMOS with an F160W filter (Mulchaey 2001). The integration time of the image is 360 s. The deprojection of the image was made by using the disk inclination of 23° (Benedict et al. 1996). We adjust the contrast of the image to get the most clear picture of the nuclear features. We see clearly that the nuclear ring of NGC 4314 is a nuclear spiral that consists of young stellar clusters of newly formed massive stars and dust lanes. The dust lanes of the spiral pattern extend further than the spiral arms and obscure some parts of the nuclear ring. The diameter of the nuclear ring is $\sim 16''$. It is elongated close to the bar axis, which is indicated by the dotted line in Figure 1. Note, however, that they are not perfectly aligned, $\Delta\theta \approx 10°$. We plot the major axis of the disk as a solid line for comparison.

Along with the nuclear ring, there seems to be an oval or a nuclear bar at the center of the galaxy (Benedict et al. 1992, 1993). The first estimate of the diameter of the nuclear bar is about $3''$ (Benedict et al. 1992), but Benedict et al. (1996) adopted the diameter of the nuclear bar as $8''$ from the *HST* image of NGC 4314 (Benedict et al. 1993). To analyze the geometrical properties of the nuclear features, we applied an ellipse fitting to the isophotes of the deprojected image of NGC 4314. Figure 2 shows the profiles of the luminosity, ellipticity, and position angle of the nuclear region of NGC 4314. The luminosity profile, which is dominated by the $r^{1/4}$ law bulge, is very smooth except for the regions affected by the dust lanes and the nuclear ring. The nuclear bar contributes an appreciable amount of luminosity, which makes a shallow gradient from $r \approx 4''$ to the end of the nuclear bar. As indicated in Figure 2, the nuclear bar ends at $r \approx 5''.2$, and the locations of the dust lanes and the nuclear ring are $\sim 7''$ and $\sim 8''$, respectively. Our estimate of the nuclear bar length agrees with that of Benedict et al. (1996), if we take into account the projection effect.

As shown in Figure 2, the nuclear bar and the nuclear ring show an excess of luminosity above the bulge luminosity, while the dust lanes show a deficiency of luminosity. The gradual increase of the ellipticity within $r \approx 5''.5$ is due to the nuclear bar. The complicated variation of the ellipticity profile reflects the complex structure of the nuclear region. The ellipticity of the nuclear ring is about 0.35, which is slightly larger than that of the dust lanes. The position angles of the nuclear features are very similar, with $\Delta\theta \lesssim 5°$.

Although the presence of a nuclear bar inside the nuclear ring of NGC 4314 has been suggested (Benedict et al. 1992, 1993, 1996), its morphology is not known yet because of the dominant bulge luminosity. To see the nuclear bar more clearly, we subtracted the axisymmetric bulge component from the deprojected image of NGC 4314 by assuming that the bulge luminosity follows the de Vaucouleurs's $r^{1/4}$ law. To do this, we derived the effective brightness and effective radius of NGC 4314 from the minor-axis profile, which is affected little by the luminosity of the nuclear bar. Figure 3 shows the bulge-subtracted image of the nuclear region of NGC 4314 where we see clearly the nuclear bar, which aligns almost parallel to the nuclear ring. We plot an ellipse

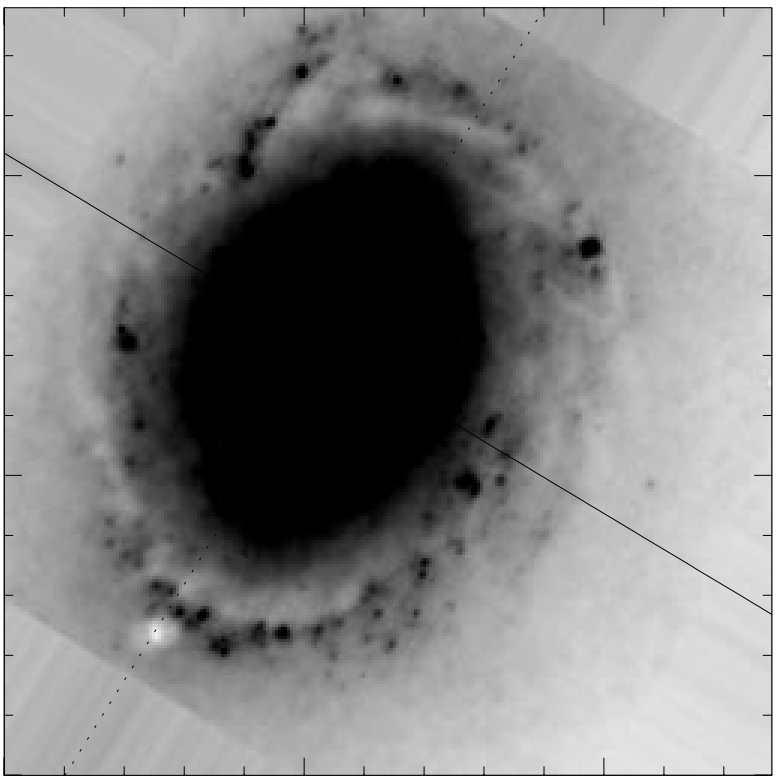


FIG. 1.—Deprojected *HST* NICMOS image of NGC 4314. We see that the nuclear ring of NGC 4314 is a nuclear spiral that consists of young stellar populations and dust lanes. The dust lanes of the spiral pattern extend further than the spiral arms and obscure some parts of the nuclear ring. The nuclear ring is elongated close to the major axis of the primary bar, which is indicated as a dotted line. The direction of the major axis of the disk is shown by a solid line. The oval shape inside the nuclear ring is due to a nuclear bar, which aligns almost parallel to the nuclear ring. The image size is $19''.2 \times 19''.2$. North is up, and east is to the left.

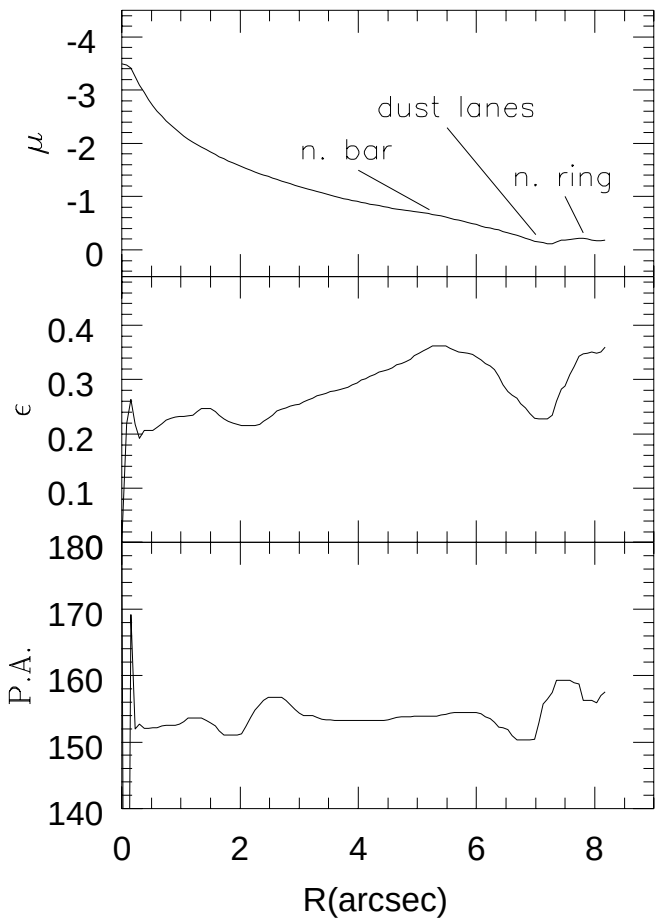


FIG. 2.—Luminosity, ellipticity, and position angle profiles of the nuclear region of NGC 4314. The luminosity profile is dominated by the bulge luminosity, but the nuclear bar contributes an appreciable amount of luminosity that makes a shallow gradient from $r \approx 4''$ to the end of the nuclear bar at $r \approx 52$. We designate the locations of the end of the nuclear bar, the dust lanes, and the nuclear ring. The gradual increase of the ellipticity within $r \approx 5''.5$ is due to the nuclear bar. The position angles of the nuclear features are similar, but the small mismatch ($\Delta\theta \approx 5°$) between the orientations of the nuclear bar and the nuclear ring is worth noting.

whose ellipticity and position angle are determined from the ellipse fitting employed in Figure 2. We see that the ellipse fits the nuclear ring nicely. The brightest hot spots outside the ellipse belong to the nuclear spiral arms.

3. MODELS

The basic numerical method employed in the present study is the SPH technique, which is known to be a powerful tool for a wide variety of astrophysical problems (see Monaghan 1992 for a thorough review). We used the same code as that of Ann & Lee (2000). We simulate the responses of a gaseous disk by having the SPH particles distributed uniformly in the beginning of each simulation, with circular velocities for the centrifugal equilibrium to the gravitational accelerations. The initial radius of the gaseous disk is 4.5 kpc. The number of SPH particles is around 10,000, which gives an initial resolution length of about 130 pc. Throughout the calculations, we fixed the temperature of the gaseous disk at 10,000 K, because radiative cooling is effective in the shocked gas. For simplicity and better resolution, our calculations were confined to a two-dimensional disk.

3.1. *The Potential*

We assumed that the galactic potential, which is due to three stellar components (bulge, disk, and bar) and the dark halo, is independent of time in the frame corotating with the bar. We include the dark halo to match the observed flat rotation curve in the outer part (Combes et al. 1992). We have performed model simulations with and without a nuclear bar to see the effect of the nuclear bar on the response of gaseous disk. We used the same functional forms of the potentials of disk, bulge, bar, and dark halo as those of Lee et al. (1999). In brief, we assumed the exponential disk (Freeman 1970), Plummer's model, the biaxial potential of Long & Murali (1992), and the logarithmic potential for disk, bulge, bar, and dark halo, respectively. We add the bar potential slowly over half a bar revolution ($\tau_{\rm bar} \approx 10^8$ yr) to avoid the violent shocks due to a sudden nonaxisymmetric force. We ignore the self-gravity of the gaseous disk because its mass is assumed to be a small fraction of the total mass of the model galaxy. The effect of self-gravity is most pronounced in the central region, where the density of SPH particles is high because of the bar-driven inflow (Ann & Lee 2000).

3.2. *Model Parameters*

The free parameters that define the gravitational potential of each component can be constrained by the mass distributions inferred from the luminosity distributions of NGC 4314. We derived the mass fractions and scale lengths of the disk, the bulge, and the bar from the results of a profile decomposition of the V-band surface photometry (Ann 1999). Here we assumed a constant mass-to-luminosity ratio throughout the galaxy. Only exception to this is the bulge scale length, because there is no direct match between the scale parameters of the adopted functional form for the bulge potential and those of the assumed function of the bulge luminosity distribution. We also assumed a large extended halo, whose mass inside the bar radius is about 10% of the visible mass. The length of the nuclear bar is assumed to be $\sim 10''$ with its axial ratio of 4. We have assumed the mass of the nuclear bar as 2% of the primary bar, based on its size.

The pattern speed of the bar Ω_p is constrained by the resonance locations and the maximum rotational velocity that is determined by the radius and mass scale of the galaxy. The length scale of our models is taken as the radius of the bar, $R_{\rm sc} = 3$ kpc, assuming the distance of NGC 4314 is 10 Mpc. We assumed that the total visible mass within the bar radius is $2 \times 10^{10}\ M_\odot$, which is about 10 times larger than the total mass interior to $r = 450$ pc (García-Barreto et al. 1991) and one-fourth of the dynamical mass of NGC 4314 (Sage 1993). We assumed the mass of the gaseous disk as 1% of the total visible mass, $M_g = 2 \times 10^8\ M_\odot$, which is virtually the same as the mass of molecular gas ($2.1 \times 10^8\ M_\odot$) derived by Benedict et al. (1996). With these radius and mass scales, the dynamical timescale $\tau_{\rm dyn}$ is 1.7×10^7 yr, and the unit of angular frequency $\Omega_{\rm sc}$ is 56.6 km s^{-1} kpc^{-1}. Assuming that the bar ends near corotation ($R_{\rm CR} \approx 1.2R_{\rm bar}$), we determined the pattern speed of the bar as $\Omega_p = 33.6$ km s^{-1} kpc^{-1}, which corresponds to $0.6\Omega_{\rm sc}$. Our bar pattern speed is almost the same as that derived by the resonance model of García-Barreto et al. (1991). We list the adopted parameters of the models in Table 1. The A model does not have a nuclear bar, while the B and C models have a synchronous nuclear bar and a fast nuclear

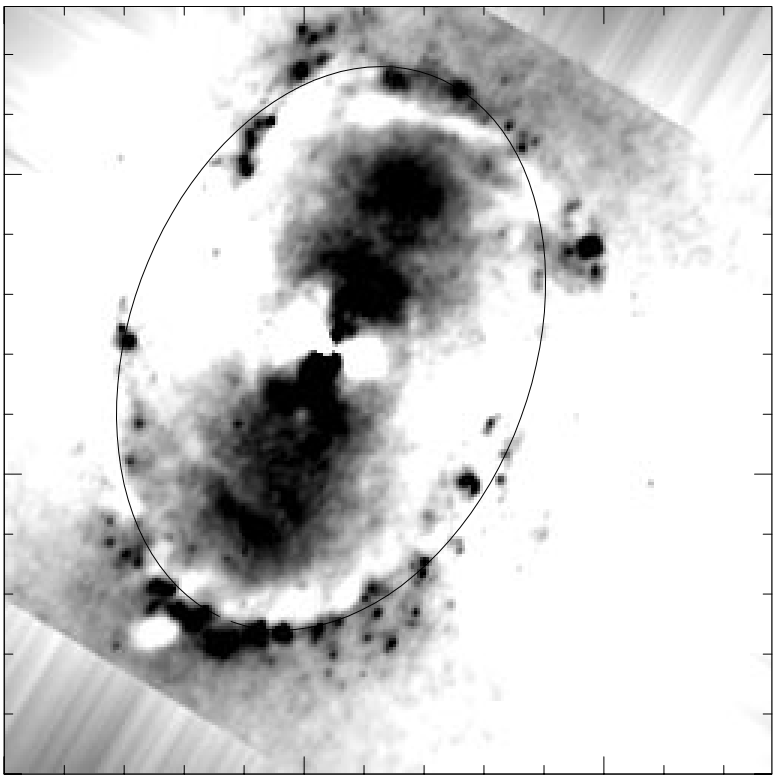


FIG. 3.—Deprojected and bulge-subtracted image of the nuclear region of NGC 4314. We see clearly a nuclear bar inside the nuclear ring. We plot an ellipse that was derived from the ellipse fit employed in Fig. 2. Most of the hot spots, which are thought to consist of the nuclear ring, are located along the ellipse. We adjust the display level to see the nuclear features most clearly. The image size is 19″.2 × 19″.2. North is up, and east is to the left.

bar, respectively. The pattern speed of the fast nuclear bar was adopted as $\Omega_s \approx 12\Omega_p$ to ensure that the CR of the nuclear bar coincides with the location of the inner inner Lindblad resonance (IILR) of the primary bar.

Figure 4 shows the rotation curve and angular frequencies of the simplest mass model (A model). The shape of the rotation curve is similar to those derived from the *K*-band image (Combes et al. 1992) and the CO observations (Benedict et al. 1996). However, our rotation curve rises somewhat more slowly than those of Combes et al. (1992) and Benedict et al. (1996), but it rises more steeply than that of Quillen, Frogel, & González (1994), which is obtained from a mass model based on a *K*-band image. The maximum rotational velocity of the model galaxy is about 180 km s^{-1}, which is in a good agreement with Combes et al. (1992) and Benedict et al. (1996). We indicated the resonance locations in Figure 4, in which IILR, OILR, and OLR stand for the inner inner Lindblad resonance, the outer inner Lindblad resonance, and the outer Lindblad resonance, respectively. The pattern speed of the bar is represented as the dot-dashed line. Because the mass of the nuclear bar is assumed to be negligible, the rotation curves of the models with nuclear bars (B and C model) are virtually the same as that of the simplest model. The rotation curves of our mass models result in a general agreement between the locations of the IILR of the model galaxies and the observed radius of the nuclear ring of NGC 4314.

4. RESULTS

4.1. *Evolution of Global Morphology*

Since the global morphological evolutions of the gaseous disk of the models with and without nuclear bars are very similar, we present the evolution of the simplest model, which has no nuclear bar (A model), in Figure 5 to see the general gas responses that lead to the development of a nuclear ring, dust lanes, and faint outer spiral arms. The number in the top left corner of each panel represents the evolution time in units of bar revolution time $\tau_{\rm bar}$, which corresponds to $\sim 6.4\tau_{\rm dyn}$. In the early phase of evolution, a two-armed spiral pattern of density enhancement is developed in the gaseous disk because of bar forcing, which drives the gas-streaming motion. The gas inside the CR moves inward by losing its angular momentum to the bar,

TABLE 1

MODEL PARAMETERS

Model	M_g	r_h	r_d	r_b	a	b	Ω_p	M_d	M_b	$M_{\rm bar}$	M_s	a_s	b_s	Ω_s
A.....	0.01	3.0	1.0	0.17	1.0	0.25	0.6	.34	.35	.30	...	...	...	...
B.....	0.01	3.0	1.0	0.17	1.0	0.25	0.6	.34	.35	.30	0.005	0.08	0.02	0.6
C.....	0.01	3.0	1.0	0.17	1.0	0.25	0.6	.34	.35	.30	0.005	0.08	0.02	7.0

NOTE.—The parameters of the nuclear bars are designated by the subscript "*s*."

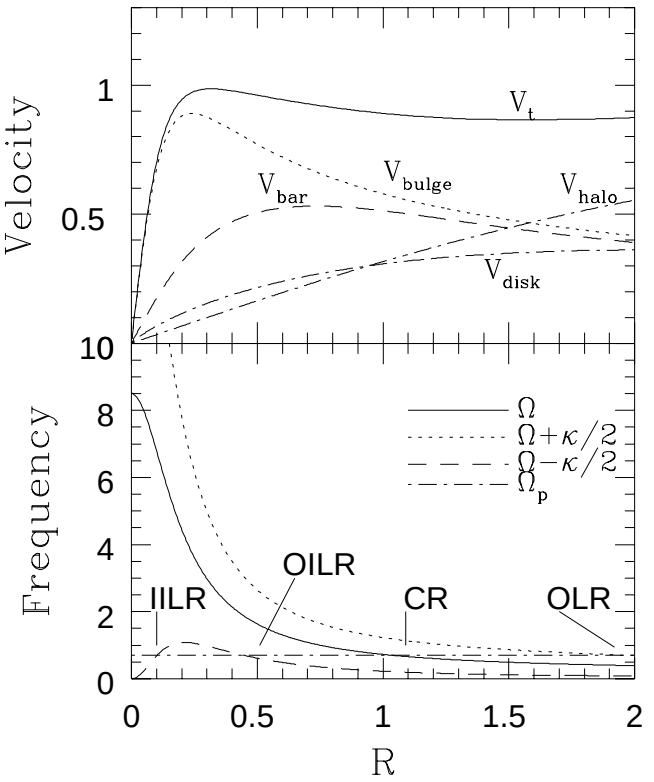


FIG. 4.—Rotational velocity and angular frequencies of the mass models of NGC 4314. The mass fractions and the scale lengths are constrained by the results of the profile decomposition (Ann 1999). The horizontal line represents the bar pattern speed Ω_p, which is determined by the assumption of $R_{CR} \approx 1.2R_{bar}$. We indicate the four resonance positions. The unit of R is 3 kpc, and the units of the velocity and the angular frequency are 170 km s^{-1} and 56.6 km s^{-1} kpc^{-1}, respectively.

while the gas outside the CR moves outward by gaining angular momentum from the bar. The spiral pattern inside the CR transforms into a perpendicular nuclear ring near OILR with highly curved symmetric dust lanes within one bar revolution. While the misalignment of the nuclear ring is decreasing and the dust lanes become less curved, the outer spiral arms extend farther. The dust lanes eventually turn into centered straight dust lanes by the time the nuclear ring aligns with the bar, after $\sim 2\,\tau_{bar}$.

As the evolution proceeds, the dust lanes become weaker, and the size of the nuclear ring decreases with increasing density until they reach a steady state after $\sim 8\,\tau_{bar}$. The location and morphology of the nuclear ring after $\sim 5\,\tau_{bar}$ resembles those of the nuclear ring of NGC 4314. The faint outer arms are reminiscent pseudo outer rings R' observed in barred galaxies (Buta 1995). Most of the gas within the CR is accumulated in the nuclear ring at the IILR, but some fraction of the gas comes across the nuclear ring and falls into the nucleus itself.

Figure 6 shows a snapshot of the velocity field of the gaseous disk of the A model at $t = 4\,\tau_{bar}$. The arrows represent the directions of the particle velocities with the lengths being proportional to the velocities. As is evident in the figure, the SPH particles near the CR have almost zero velocity. The streaming motion of gas particles is easily seen inside the CR, where the gas particles lead the bar. The streaming motion indicates that there is a large amount of gas inflow along the bar. The velocity of inflowing gas is up to ~ 100 km s^{-1}, which agrees with the observations of Benedict et al. (1996). The outer trailing spiral arms are composed of gas particles that move outward by gaining angular momentum from the bar, while the straight dust lanes and ringlike structures are composed of gas particles that move inward by losing their angular momentum to the bar. It is also worth noting that the slightly curved leading dust lanes seen in Figure 5 are the regions of density enhancement with abrupt velocity changes. The high density and the sudden velocity changes could imply that they are the loci of shock fronts. In later times, when the evolution of the gaseous disk reaches a steady state, the streaming motion, which leads to the gas inflow toward the nucleus, is significantly reduced.

4.2. *Evolution of Nuclear Region*

Although the global morphological evolutions of the gaseous disks are not much different among models with or without nuclear bars, the evolutions of the nuclear features are quite different due to the perturbations by nuclear bars. Figure 7 shows the evolution of the central part of the gaseous disk of the models with a synchronous nuclear bar (B model) and a fast nuclear bar with $\Omega_s \approx 12\Omega_p$ (C model), along with that of the simplest model. The CR of the nuclear bar is located near the IILR of the primary bar for the C model. Because the gas responses outside the nuclear ring are almost identical in every evolution stage, we plot the nuclear regions only for better resolution. The box size of Figure 7 is 1.2 kpc in one dimension. For easy comparisons of the models with the observations, we plot the distribution of the SPH particles, with the ellipse representing the nuclear ring of NGC 4314. Because the primary bar lies along the horizontal axis in Figure 7, we rotate the ellipse accordingly.

The morphology of the inner parts is similar to each other until $\sim 2\,\tau_{bar}$, but they evolve differently afterward. The nuclear ringlike structure developed in the A model evolves to a nuclear ring after $\sim 5\,\tau_{bar}$, whose general morphology resembles the nuclear ring morphology of NGC 4314. The nuclear ring consists of several fragments of various morphology. However, the spiral pattern observed in the nuclear ring of NGC 4314 cannot be reproduced by the A model. The evolution of the B model shows a highly elongated nuclear spiral at $t \approx 2\,\tau_{bar}$ with a large accumulation of gas in the nucleus. The nuclear spiral pattern evolves to a nearly circular nuclear ring, located far inside the IILR. There is not much gas in the nuclear ring, owing to the large amount of infall to the nucleus. The steady state morphology of the nuclear ring of the B model is much different from that of NGC 4314. The nuclear ringlike structure of the C model evolves to several fragments, which distribute randomly inside the IILR. However, after $\sim 5\,\tau_{bar}$, they evolve to a two-armed spiral pattern with a large accumulation of gas near the nucleus. The morphology of the nuclear spiral at $\sim 8\,\tau_{bar}$ resembles the nuclear ring morphology of NGC 4314. However, the nuclear spiral developed in the C model is a transient one. Moreover, NGC 4314 has no nuclear structure similar to that developed in the nucleus of the C model.

There are some similarities in the evolution of the nuclear morphologies among the models. All the models show the shrinking of the nuclear rings with the increasing of the gas density inside because of the gas inflow toward the nucleus. However, as evident from Figure 7, while most of the gas inside the CR is accreted between the two ILRs in the

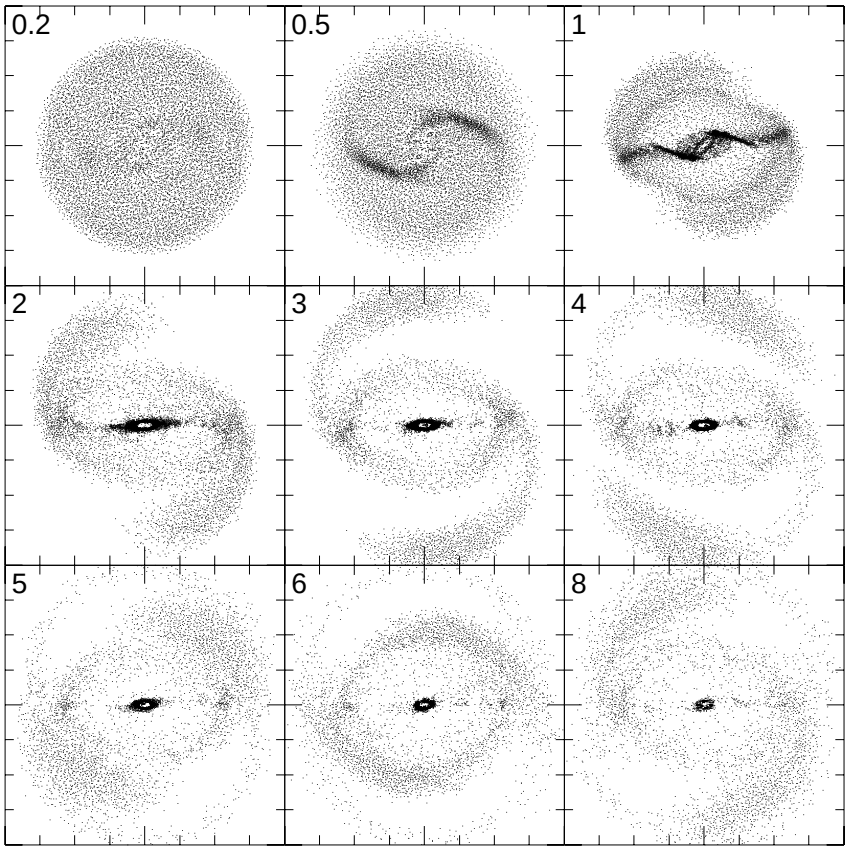


FIG. 5.—Evolution of the gaseous disk of the simplest model (A model). At earlier times the nuclear ring shows a large misalignment with the bar but becomes aligned parallel to the bar after $\sim 3\ \tau_{bar}$. The diameter of the nuclear ring decreases as it evolves. The number of each panel is the evolution time in units of τ_{bar} ($\sim 1.1 \times 10^8$ yr). It reaches to the steady state after $\sim 8\ \tau_{bar}$. The bar lies horizontally. The box size is 12 kpc in one dimension.

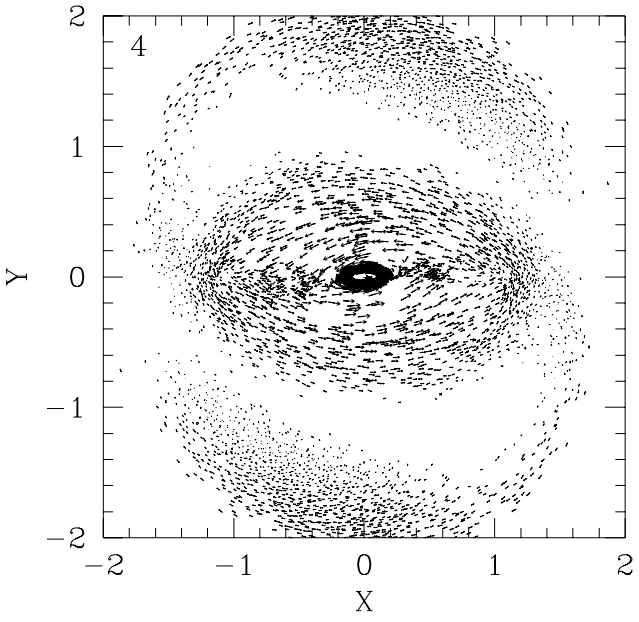


FIG. 6.—Velocity field of A model at $t = 4\ \tau_{bar}$. The lengths of arrows are proportional to the particle velocities. The particles inside the corotation radius show strong streaming motions along the bar. See the abrupt change of the particle velocity near the bar axis, which might represent the loci of the shock fronts. The length is 3 kpc for both axes.

A model, a large fraction of the gas inside the CR moves into the nucleus after $\sim 2\ \tau_{bar}$ in the B model and after $\sim 3\ \tau_{bar}$ in the C model, respectively. One interesting point to be noted is the development of several fragments that are thought to be the regions of density enhancement. Since there is no common property in the structures of the fragments, they might be caused by some sort of dynamical instability due to random shocks.

5. DISCUSSION

5.1. *Orientation of Nuclear Ring*

Most of the nuclear rings observed in real galaxies are misaligned, usually perpendicular to the primary bars (Buta & Crocker 1993). Thus, the nuclear ring of NGC 4314, which is elongated to the direction nearly parallel to the bar axis, with an ellipticity of $\epsilon \sim 0.35$, is a rare example of aligned nuclear rings. The misalignment angle of the nuclear ring with the primary bar is only $\sim 10°$. It is well known that the morphology of nuclear rings depends on the dynamical properties of the host galaxies, such as mass distribution and bar pattern speed. The dependence of the nuclear ring morphology on the bar pattern speed was examined by Combes & Gerin (1985), who showed that slow bars induce elongated nuclear rings aligned parallel to the bar, while fast bars that allow only one ILR generate circular nuclear rings.

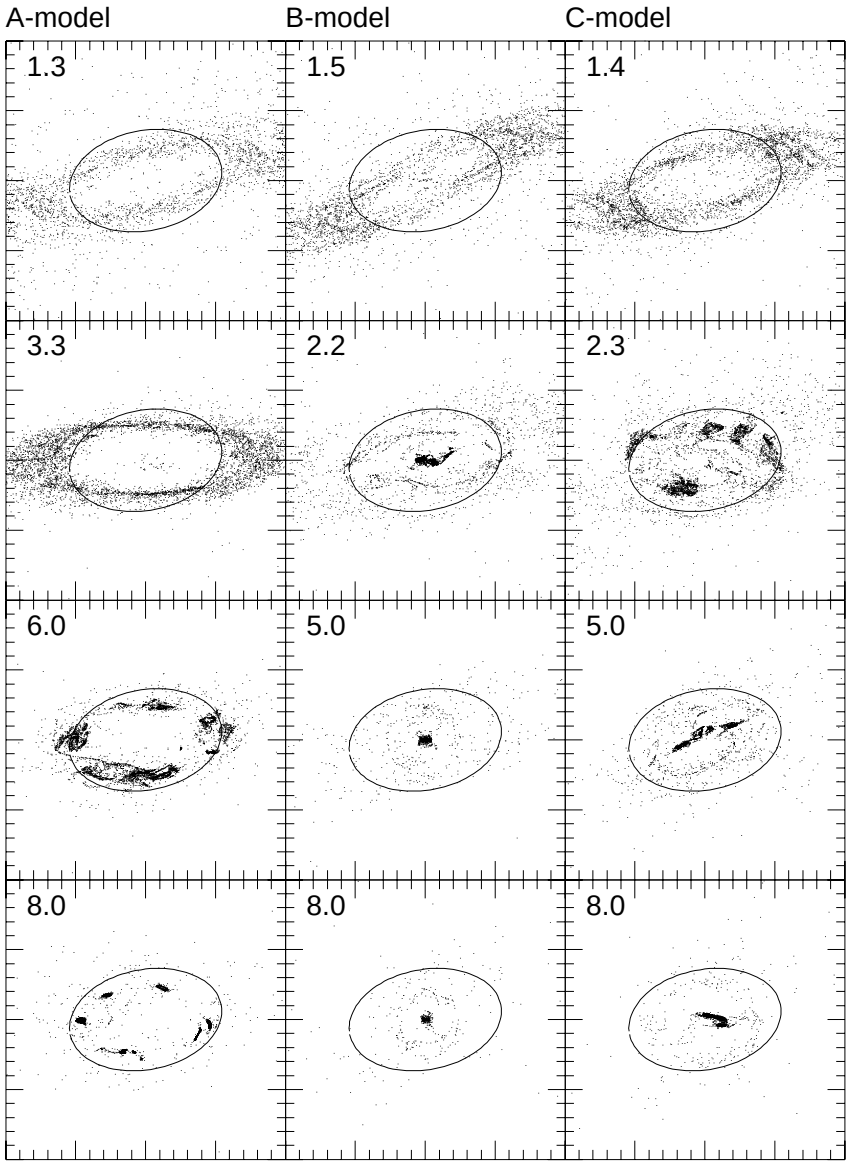


FIG. 7.—Evolution of the nuclear region of three models. The A model has no nuclear bar, and the B- and C models have a synchronous nuclear bar and a fast nuclear bar ($\Omega_s \approx 12\Omega_p$), respectively. The ellipse that represents the nuclear ring of NGC 4314 is plotted for easy comparison. Because the primary bar lies horizontally, we rotate the ellipse accordingly. We see that there is no spiral pattern in the A model, while the B and C models show a nuclear spiral pattern, at least in some stages of evolution. Note that the nuclear bars induce much infall into the nucleus. The number of each panel represents the evolution time in units of $\tau_{\rm bar}$. The box size is 1.2 kpc in one dimension.

However, there does not seem to be much freedom for the pattern speed of a bar because it ends near the CR (Contopoulos 1980; Athanassoula 1992). A more important parameter that constrains the morphology of nuclear rings is the degree of central mass concentration (Piner et al. 1995; Ann & Lee 2000). Piner et al. (1995) showed that galaxies with high central concentrations and small bar axial ratios have circular nuclear rings, while galaxies with low central concentrations and large axial ratios have elongated nuclear rings that tend to be aligned with the bars. The nuclear rings of galaxies that have strong bars with axial ratios of $a/b \gtrsim 4$, however, can be aligned perpendicular to the bar if the central concentration is very high (Ann & Lee 2000). Thus, the central concentration of mass distribution seems to be the primary parameter that controls the nuclear ring morphology. The aligned nuclear ring of NGC 4314 is due to the strong bar with a moderate degree of central concentration of mass.

The central concentration is not an observable quantity, but it can be inferred from the rising part of the rotation curve, which is mainly determined by the mass distribution of the bulge component. Centrally concentrated bulges give rise to steep rotation curves, which allow two ILRs unless the bar pattern speed is unrealistically high. This is the reason for the preponderance of occurrences of nuclear rings in early-type galaxies (Buta & Crocker 1993). In the present mass models, the rising part of the rotation curve strongly depends on the bulge scale length r_b in the Plummer spherical potential. We adopted the bulge scale $r_b = 510$ pc, which is slightly larger than that used by García-Barreto et al. (1991), who modeled NGC 4314 using a Plummer spherical bulge and a Toomre disk with a bulge scale length of 400 pc.

5.2. *Shrinking of Nuclear Ring*

One interesting phenomenon observed in the evolution of

the nuclear morphology is the shrinking of ringlike structures, which are formed near the OILR. Their sizes are reduced as much as the ratio of $R_{\rm OILR}$-to-$R_{\rm IILR}$. Such a shrinking is not a common property of nuclear ring evolution. It requires an extremely strong nonaxisymmetric potential by which the particles populating the aligned nuclear ring lose angular momentum because of the gravitational torque. Misaligned nuclear rings or aligned nuclear rings with weak bars do not show such a shrinking (Ann & Lee 2000). The strong nonaxisymmetric potential of NGC 4314 is provided by the large axial ratio ($a/b \approx 4$) and the high-mass fraction ($\sim 30\%$) of the primary bar.

Shrinking of the nuclear ring of NGC 4314 is suggested by Combes et al. (1992) from the location of the molecular ring, observed by a high-resolution CO ($J = 1$–0) mapping of NGC 4314. They interpreted the mismatch of the locations of the radio ring and the molecular ring as a result of the shrinking of the molecular ring, which is located inside the radio ring. The position of the radio ring coincides with the optical nuclear ring. However, the timescale for the shrinking of the molecular ring is very short, comparable to the star formation timescale of a few 10^7 yr (Combes et al. 1992). In the models with nuclear bars, the ringlike structures formed at the OILR shrink to the IILR in a few 10^8 yr, while in the model with no nuclear bar, the shrinking timescale is about 10^9 yr.

The slow shrinking of the nuclear ring, as compared with the star formation timescale, indicates that the mean age of the stellar populations in the nuclear region changes with radius, older in age near the OILR and younger in age near the IILR, if the nuclear ring of NGC 4314 has evolved from the ringlike structure formed near the OILR. Thus, the variation of stellar colors, progressively becoming redder with increasing distance from the nuclear ring, observed by Benedict et al. (1992) can be explained by the age difference of the stellar populations, as suggested by Benedict et al. (1996).

5.3. *Pattern Speed of Nuclear Bar*

As shown in Figure 3, there seems to be no question about the presence of a nuclear bar inside the nuclear ring of NGC 4314. Its morphology is similar to that of the primary bar. However, there is no information about the dynamical properties of the nuclear bar, except for the small misalignment between the two bars, $\Delta\theta \approx 5^\circ$. In a double-barred system, from a dynamical point of view, a favorable situation consists of a faster nuclear bar with its CR at the location of the ILR of the primary bar, when the primary bar ends near the CR of the primary bar (Pfenniger & Norman 1990; Friedli & Martinet 1993). However, in the case of NGC 4314, there is a possibility of a synchronous rotation because of the virtual alignment of the two bars (Benedict et al. 1996).

However, as evident from Figure 7, the evolution of the gas response inside the OILR depends sensitively on the pattern speed of the nuclear bars. The model with a fast nuclear bar drives a complicated evolution that leads to the formation of a two-armed nuclear spiral, resembling the nuclear ring of NGC 4314, while the model with a synchronous nuclear bar develops a smaller and rounder nuclear ring than that of NGC 4314. The spiral pattern developed in the early phase of evolution in the model with a synchronous nuclear bar is very short lived and highly elongated. Thus, the nuclear bar of NGC 4314 is thought to rotate faster than the primary one. We might observe the nuclear bar, when it lies close to the primary bar. However, since there is little gas in the nucleus of NGC 4314 (García-Barreto et al. 1991), there should be some mechanisms that remove the infalled gas inside the nuclear ring, if the nuclear structure of NGC 4314 can be explained by the models with a fast nuclear bar.

6. CONCLUSIONS

The peculiar nuclear morphology of the early-type, strongly barred galaxy, NGC 4314, can be explained by dynamical models, in which mass models are constrained by the results of profile decomposition and the assumption of $R_{\rm CR} \approx 1.2R_{\rm bar}$ for the bar pattern speed. Our SPH simulations reproduce well the shape and orientation of the nuclear ring of NGC 4314, which is characterized by an elongated ring and spiral arms of young stellar populations, partly obscured by the dust lanes and aligned nearly parallel to the bar ($\Delta\theta \approx 10^\circ$). The aligned nuclear ring of NGC 4314 can be formed from the gas inflow along the bar because of the moderate central concentration of the bulge under the strong barred potential. The constraints of the location of the nuclear ring at the IILR ($R_{\rm IILR} \approx 350$ pc) and the bar ending near the CR admit a slow rotation of the bar ($\Omega_p \approx 34$ km s^{-1} kpc^{-1}), which is effective for the mass inflow toward the nucleus.

We have presented the results of three SPH simulations with different assumptions about the nuclear structure: no nuclear bar, a synchronous nuclear bar, and a fast nuclear bar. There is little difference in the evolutions of the global morphology among the models, but the evolutions of nuclear morphology are quite different because of the different nuclear dynamics. In the beginning of the evolution of the gaseous disks, the nuclear ring forms from the density enhancement of spiral pattern, which is originated from the streaming motions due to the gravitational torque on the gas. At the time of nuclear ring formation, it is aligned perpendicular to the primary bar, but the misalignment angle decreases after one bar revolution. The diameter of the nuclear ring decreases as the inflowing gas accumulates in the IILR, with the gradual disappearance of dust lanes along the bar.

If there is no nuclear bar, the nuclear spiral pattern similar to that of NGC 4314 cannot be developed, even though the general morphology of the nuclear ring located near the IILR resembles the nuclear ring of NGC 4314. The synchronous nuclear bar drives a large infall into the nucleus and develops a highly elongated nuclear spiral at earlier times, which evolves to a circular nuclear ring far inside the IILR after $\sim 5\,\tau_{\rm bar}$. The steady state morphology induced by the synchronous nuclear bar is much different from the observed one. In the case of the model with a fast nuclear bar ($\Omega_s \approx 12\Omega_p$), the evolution of the nuclear feature is very complicated because of the fluctuating potential by the fast nuclear bar. However, it leads to the formation of a nuclear ring of spiral pattern that resembles the observed nuclear ring of NGC 4314. Thus, the nuclear bar of NGC 4314 seems to rotate faster than the primary bar. The small misalignment between the two bars, $\Delta\theta \approx 5^\circ$ might indicate that we see the nuclear bar of NGC 4314 when it lies close to the primary bar. However, there should be some mechanisms by which the infalled gas is removed from the nucleus if the nuclear morphology of NGC 4314 can be explained by the nuclear dynamics induced by the fast nuclear bar.

I thank Hyesung Kang for the help in the numerical work and Hyung Mok Lee for careful reading of the manuscript and discussion. I would like to thank J. Mulchaey for providing me the *HST* NICMOS image of NGC 4314 before publication. I want to thank the anonymous referee for the kind comments by which this paper is much improved. This work was supported by the Interdisciplinary Research Program of KOSEF through grant 1999-2-113-001-5.

REFERENCES

Ann, H. B. 1999, J. Korean Astron. Soc., 32, 83
Ann, H. B., & Lee, H. M. 2000, J. Korean Astron. Soc., 33, 1
Athanassoula, E. 1992, MNRAS, 259, 345
Benedict, G. F. 1980, AJ, 85, 513
Benedict, G. F., et al. 1993, AJ, 105, 1369
Benedict, G. F., Higdon, J. L., Tollestrup, E. V., Hahn, J., & Harvey, P. M. 1992, AJ, 103, 757
Benedict, G. F., Smith, B. J., & Kenny, J. D. P. 1996, AJ, 111, 1861
Burbidge, E. M., & Burbidge, G. R. 1962, ApJ, 135, 694
Buta, R. 1995, ApJS, 96, 39
Buta, R., & Crocker, D. A. 1993, AJ, 105, 1344
Combes, F. 1996, in IAU Colloq. 157, Barred Galaxies, ed. H. L. Morrison & A. Sarajedini (ASP Conf. Ser. 91; San Francisco: ASP), 286
Combes, F., & Gerin, M. 1985, A&A, 150, 327
Combes, F., Gerin, M., Nakai, N., Kawabe, R., & Shaw, M. A. 1992, A&A, 259, L27
Contopoulos, G. 1980, A&A, 81, 198
Freeman, K. C. 1970, ApJ, 160, 811
Friedli, D., & Martinet, L. 1993, A&A, 277, 27
Gallagher, J. S., Faber, S. M., & Balick, B. 1975, ApJ, 202, 7
García-Barreto, J. A., Downes, D., Combes, F., Gerin, M., Megri, C., Carrasco, L., & Cruz-Gonzalez, I. 1991, A&A, 244, 257
Lee, C. W., Lee, H. M., Ann, H. B., & Kwon, K. H. 1999, ApJ, 513, 242
Long, K., & Murali, C. 1992, ApJ, 397, 44
Lynds, B. T. 1974, ApJS, 28, 391
Lynds, B. T., Furenlid, I., & Rubin, J. 1973, ApJ, 182, 659
Monaghan, J. J. 1992, ARA&A, 30, 543
Mulchaey, J. 2001, in preparation
Pfenniger, D., & Norman, C. 1990, ApJ, 363, 391
Piner, B. G., Stone, J. M., & Teuben, P. J. 1995, ApJ, 449, 508
Quillen, A. C., Frogel, J. A., & González, R. A. 1994, ApJ, 437, 162
Sage, L. J. 1993, A&A, 272, 123
Sandage, A. 1961, The Hubble Atlas of Galaxies (Washington: Carnegie Inst. Washington)
Schwarz, M. P. 1981, ApJ, 247, 77
———. 1984, MNRAS, 209, 93
Wakamatsu, K., & Nishida, M. T. 1980, PASJ, 32, 389